forum acusticum 2026
8-12 September · Graz, Austria

ROBUSTNESS OF RAINBOW TRAPPING SILENCERS TO LOW-SPEED FLOW EFFECTS

Cédric Maury[1], Teresa Bravo[2], Daniel Mazzoni[3], Cédric Pinhède[1]

[1] *Laboratory of Mechanics and Acoustics (LMA CNRS UMR 7031), Marseille, France*

[2] *Spanish National Research Council (CSIC), Madrid, Spain*

[3] *Institute of Research on Non-Equilibrium Phenomena (IRPHE CNRS UMR 7342), Marseille, France*

This paper is a revised version of the authors' submitted manuscript that was peer-reviewed by at least two anonymous reviewers.

Abstract

This study investigates the aero-acoustic robustness of rainbow trapping structures (RTSs) with straight and coiled cavities in fully opened and flow-compliant convergent configurations under a low-speed grazing flow. A transfer matrix model is developed to predict dissipation and transmission loss (TL), and validated against finite element simulations of the Linearized Navier–Stokes equations in the no-flow and flow cases. In the absence of flow, increasing the acoustic path length, particularly in convergent designs, broadens and downshifts the high-dissipation plateau through merging of quarter-wave resonances and improved impedance matching. The convergent straight (CS) and coiled (CC) RTSs exhibit the widest efficiency bandwidths, while the CS configuration provides the highest TL peak. All configurations remain robust under low-speed grazing flow. Upstream flow conditions (UPC) enhance attenuation relative to downstream flow conditions (DPC), yielding broader dissipation bandwidths and higher TLs, whereas DPC induce over-damping at the cavity mouths and reduced performance. In convergent designs, geometric acceleration of the flow increases the flow-induced modification of the cavity impedances. It triggers a low-frequency axial half-wavelength resonance that scales on the reduced sound speed. Overall, RTS performance is maximized in suction mode, confirming their robustness for flow-integrated noise control.

Keywords: *rainbow trapping silencers, sound dissipation, low-speed flow, transfer matrix.*

Corresponding author: *cedric.maury@centrale-marseille.fr.*

1. Introduction

A large number of studies on acoustic metamaterials focused on broadband absorption towards low-frequencies using deep sub-wavelength one-port absorbers [1,2] or two-port graded resonators [3] in a static fluid domain. A fewer number of works have addressed the properties of flush-mounted meta-liners to enhance sound attenuation at low frequencies when traversed by a low-speed flow. This problem is critical in ventilation systems for buildings and vehicles, but also for aircraft engine liners, where low-frequency sound sources become prominent. It was shown that the attenuation through thin meta-liners with folded sidebranch was reduced by 50% (resp. 20%) under downstream (resp. upstream) flow conditions at Mach 0.2, but occurs over a wider bandwidth [4]. A metaliner with C-shaped enclosures and embedded microperforates could provide a 10.2 dB average transmission loss over the bandwidth 400 Hz – 1400 Hz at Mach 0.09 [5]. Moreover, resilience of sidebranch arrays made up of graded quarter-wave cavities to flow-induced “lock-on” tones, that manifest as negative transmission coefficient, was found to be enhanced if the shorter cavities are located upstream of the deeper ones up to Mach 0.05 [6].

Most of the works on meta-liners focus on wideband sound attenuation under a low-speed flow. The current work shows the influence of a low-speed flow on the transmission, but also on the dissipation properties of a graded distribution of quarter-wave resonators that constitutes a Rainbow-Trapping Silencer (RTS). Low-frequency performance is achieved through coiled cavities and/or RTS with a convergent profile that increase the acoustical path length in the cavities.

A cost-efficient transfer matrix formulation is described in Sec. 2 to calculate the dissipative and reactive properties of RTSs that accounts for flow alteration of the cavity mouth impedance. The acoustical performance of coiled and convergent RTSs are compared in Sect. 3 in the no-flow case and assessed against finite element results. Section 4 discusses the robustness of coiled and/or convergent RTSs performance to upstream and downstream low-speed flow conditions. The main outcomes and perspectives are summarized in Sect. 5.

2. Transfer matrix formulation

A general configuration is that of an axisymmetric convergent RTS of radius $r(z)$, length L, made up of N cavities of width w with coiling (d without coiling), separated by ribs of thickness t, whose depths $D(z)$ increase along the axis z, as shown in Fig. 1. It is left - excited by a plane wave and undergoes downstream (resp. upstream) propagation conditions at Mach number $M(z) = U(z)/c_0$, associated to the blue (resp. red) arrows in Fig. 1, with $U(z)$ the mean flow speed and c_0 the sound speed. Note that $M(z)$ increases as z increases through the RTS according to mass flow rate conservation. Axial variation of the inner radius $r(z)$ complies with the design of low-speed wind tunnel sections [7]. Individual transfer matrices $\mathbf{T}_n$ are defined that relate the acoustic pressure and volume velocity across the n^{th} cavity-rib cell in plane wave regime considering the cells as pointwise scatterers without evanescent coupling. They read

$$\mathbf{T}_n = \mathrm{e}^{-\mathrm{j}Mk_M(d+t)} \begin{bmatrix} C_M & (\mathrm{j}Z_0/S)S_M \\ (\mathrm{j}S/Z_0)S_M & C_M \end{bmatrix} \mathbf{T}_{\text{cav},n} \quad (1)$$

with $S = \pi r^2(z)$, Z_0 the air characteristic impedance, $C_M = \cos[k_M(d+t)]$ and $S_M = \sin[k_M(d+t)]$ in the propagation matrix. k_M is the acoustic wavenumber that includes visco-thermal, convective and turbulent dispersion effects [8].

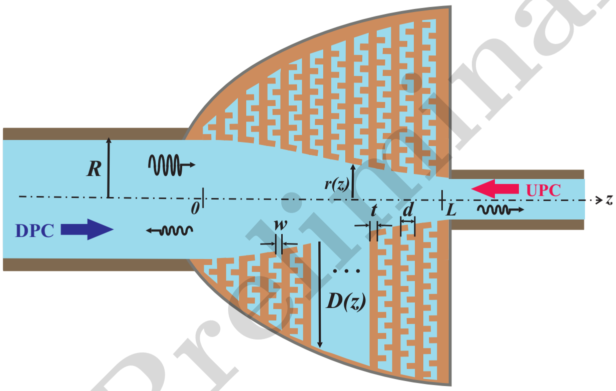

Figure 1. Sketch of a rainbow trapping silencer left-excited by a plane wave and traversed by an upstream (red) or downstream (blue) low-speed flow.

The sidebranch transfer matrix is given by

$$\mathbf{T}_{\text{cav},n} = \frac{1}{1 + 2My_n\Sigma_w} \begin{bmatrix} 1 + M\,y_n\Sigma_w & M^2 y_n^2 \Sigma_w^2 \\ S_w\,y_n/Z_0 & 1 + M\,y_n\Sigma_w \end{bmatrix} \quad (2)$$

with $\Sigma_w = 2w/\,r(z)$, $S_w = 2\pi w r(z)$ and y_n the specific input admittance of the n^{th} cavity mouth. Howe's model [9] is chosen that describes the input admittance of a rigidly-backed cavity slit under a grazing flow at low Mach number ($M < 0.3$) and with no mean shear over the cavity mouth, thereby ruling out any flow-induced instability effect. It takes the form $y_n = \left(1 - M_c H(k_c w/2)\right)/\left[y_{0,n}^{-1} - G\left(k_c w, k_c D(z_n)\right)\right]$ with $M_c \approx 0.23M$ and k_c the convective Mach number and wavenumber, $y_{0,n}$ the specific input admittance of the n^{th} annular cavity without flow [9], and the Hankel-type functions $G(u,v) = 2u/\pi + \pi^{3/2}H(u/2)\sqrt{u/v}$ and $H(u) = 1 - J_0(u)[J_0(u) - \mathrm{j}J_1(u)]^{-1}$. y_n accounts for the resistive and reactive effects of vortex shedding from the cavity upstream edge. The total transfer matrix across the RTS reads

$$\mathbf{T} = \prod_{n=1}^{N} \mathbf{T}_n \quad (3)$$

whose components lead to the left reflection and left-to-right transmission coefficients, r and t.

3. Acoustical performance of the RTSs

One considers four axisymmetric RTSs that extend over a length $L = 0.15$ m. They have an inlet radius $R = 0.04$ m associated to a duct cut-off frequency $f_c = 2511$ Hz. They are made up of $N = 40$ annular cavities separated by walls of thickness $t = 1$ mm so that the cavity width is given by $d = L/N - t = 2.7$ mm. In the fully-opened straight RTS, the axial variation of the cavity depths reads $D(z) = R(z/L)^m$ with m the rate of increase of the cavity depths set to $m = 2.5$. It ensures that the greatest cavity depth is $D(L) = R$ so that the lowest quarter-wave resonance frequency (1600 Hz) stays well below f_c. The acoustical path length within the cavities can be increased through a coiled design parametrized by a factor, $\chi = (1 + d/w)/2$, so that $D_{\text{coil}}(z) = \chi D(z)$. The coiling factor is here chosen as $\chi = 3/2$ with $w = d/2 = 1.4$ mm. A flow-compliant RTS design with a convergent radius will further increase the acoustical path length in the cavities. It is given by $D_{\text{conv-coil}}(z) = \chi\{D(z) + R - r(z)\}$ with $r(L) = \kappa R$ the outlet radius associated to a contraction factor $\kappa = 0.25$.

Figures 2 and 3 compare the dissipation and TL performance of straight (S), coiled (C), convergent straight (CS) and convergent coiled (CC) RTSs without flow for increasing acoustical path lengths of their deepest cavity at $z = L$. These indicators are simulated from the transfer matrix method (TMM) from Eqs. (1) to (3) from which the transmission coefficient, $\tau = |t|^2$, the reflection coefficient $\rho = (1-M)^2|r|^2/(1+M)^2$ and the power dissipated by the RTS, $\eta = 1 - \tau - \rho$, are obtained. The transmission loss (TL) reads $-10\log_{10}(\tau)$. The most complex CC RTS configuration is also simulated from Comsol finite element method (FEM) applied to the Linearized Navier Stokes equations with a minimum mesh size equal to one third of the viscous boundary layer at the highest frequency of interest f_c. Despite its simplifying assumptions, the TMM results show excellent agreement with respect to the FEM results, in terms of dissipation over the entire frequency range and TL up to 2.2 kHz.

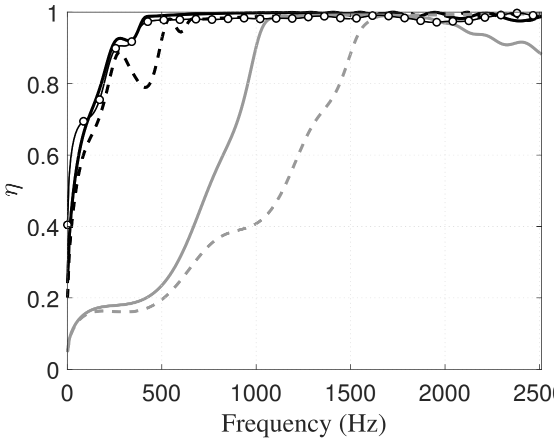

Figure 2. Dissipation spectra of a straight RTS (dashed grey), a straight RTS with coiled cavities (plain grey), a convergent RTS (dashed black) and a convergent RTS with coiled cavities (plain black) simulated by the TMM without flow; the latter case also shows FEM results (black circles).

The dissipation curves exhibit a plateau of high dissipation values that stay above 0.97 in the ranges $1600\ \mathrm{Hz} - f_c$, $1066\ \mathrm{Hz} - 1871\ \mathrm{Hz}$, $681\mathrm{Hz} - f_c$ and $426\mathrm{Hz} - f_c$, respectively for the S, C, CS and CC RTSs. This plateau behavior is due to merging of the quarter-wave resonances of the lateral cavities favored by a near-unit loss-to-leakage balance and a high impedance matching. This enables the incident wave to propagate to the axial position of the resonant cavity, in which at least 97% of its energy is dissipated through visco-thermal boundary layer effects along the cavity walls. Note that the dissipation of the CS RTS decreases down to 0.9 above 2 kHz due to over-damped cavity conditions.

A substantial progressive broadening of the efficiency range is observed, increasing from 911 Hz for the straight RTS to approximately 2 kHz for the CC RTS, spanning 4.5 octaves above 426 Hz. This downshift of the plateau onset frequency, associated to the first quarter-wave resonance frequency of the deepest cavity, is due to an increase of the acoustical path length from $D(L) = R$ for the straight RTS up to $D(L) = 2.625R$ for the CC RTS.

Consistently, Fig. 3 shows that the maximum TL values vary across configurations, reaching 64 dB (S), 35 dB (C), 86 dB (CS) and 60 dB (CC), together with progressive downshift and broadening of the TL half-bandwidth from 1.8 kHz (S), 1.2 kHz (C, CS) and 860 Hz (CC). The TL dip around 2 kHz for the CC RTS corresponds to the junction between the first-order quarter-wave resonances of the shallowest cavities with a low quality factor and the second-order quarter-wave resonances of the deepest cavities.

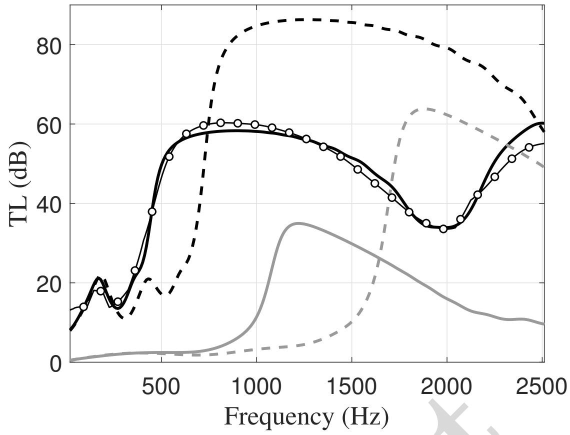

Figure 3. Transmission Loss of a straight RTS (dashed grey), a straight RTS with coiled cavities (plain grey), a convergent RTS (dashed black) and a convergent RTS with coiled cavities (plain black) simulated by the TMM without flow; the latter case also shows FEM results (black circles).

4. Aero-acoustical RTS performance

The robustness of the dissipation and TL performance of the four RTS designs are examined under downstream (resp. upstream) flow conditions, coined DPC (resp. UPC), up to $30\ \mathrm{ms}^{-1}$ ($M = 0.0875$) from TMM simulations. A coupled finite-element model was also developed to simulate turbulent flow and acoustic propagation. The low-Mach-number flow was solved using the RANS-SST turbulence model, combining the k–ω and k–ε formulations for near-wall and core-flow regions. No-slip and isothermal boundary conditions were applied at the walls. The resulting flow field was used as the background flow for an acoustic model based on Linearized Navier-Stokes Equations (LNSE) to simulate acoustic perturbations in the presence of a background acoustic field.

4.1 Fully-opened straight and coiled RTSs

Figure 4 shows that DPC upshifts by 70 Hz the near-unit dissipation plateau to higher frequencies, while UPC downshifts by 100 Hz (resp. 40 Hz) the efficiency bandwidth of straight (resp. coiled) RTSs. Grazing flow has little effect on peak dissipation, but UPC broadens and DPC narrows the dissipation bandwidth. Figure 5 further shows that UPC increases TL by up to 27 dB (straight RTS) and 5 dB (coiled RTS), while DPC reduce the maximum TLs by 15 dB and 10 dB, respectively. The TL performance predicted by the TMM are in close agreement against those obtained from the FEM coupling RANS-SST and LNSE.

The acoustical performance of the RTS is therefore enhanced under UPC compared with DPC, particularly for the straight configuration. First, this is due to an increase of the flow-induced reactance of each resonant cavity when U decreases from $30\ \mathrm{ms}^{-1}$ to $-30\ \mathrm{ms}^{-1}$. It produces a downshift and broader distribution of the cavity-duct resonance frequencies that are still able to merge at $U = -30\ \mathrm{ms}^{-1}$. Second, UPC and DPC lead to an increase of the flow resistance over the cavity mouths, which is more pronounced under DPC than UPC. At $U = 30\ \mathrm{ms}^{-1}$, this excess flow resistance results in an over-resistive loss-to-leakage ratio that lowers the dissipation of the coiled RTS above 2 kHz and alters the maximum TL values, as seen in Fig. 4 and 5. At $U = -30\ \mathrm{ms}^{-1}$, a more moderate increase of the flow-induced resistance maintains a balanced loss-to-leakage factor resulting in a near-unit dissipation plateau over a broader bandwidth and higher TL values. The higher TL values of the straight RTS compared with the coiled RTS result from a slight increase in dissipation (from 0.5% to 1%), to which the TL is very sensitive. Overall, UPC appear to enhance the dissipative and attenuation properties of both straight and coiled RTS.

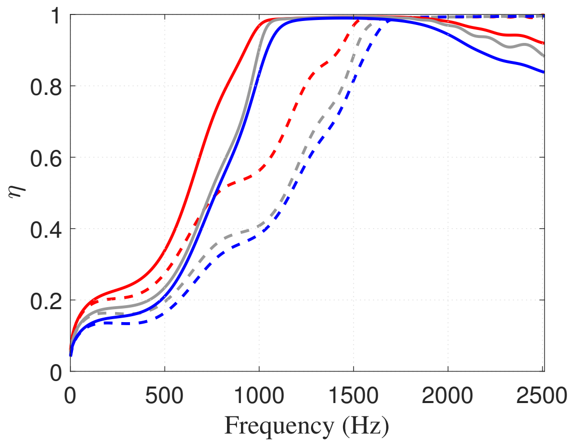

Figure 4. Influence of a low-speed flow ($U = -30\ \mathrm{ms}^{-1}$, red; $U = 30\ \mathrm{ms}^{-1}$, blue) on the dissipation spectra of a straight RTS (dashed) and a straight RTS with coiled cavities (plain) simulated by the TMM; the grey curves correspond to the no-flow case.

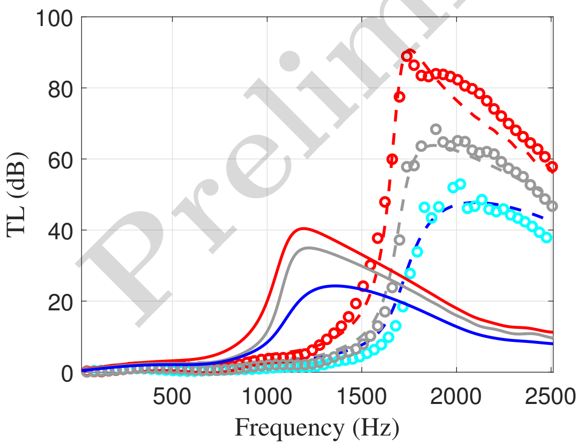

Figure 5. Influence of a low-speed flow ($U = -30\ \mathrm{ms}^{-1}$, red; $U = 30\ \mathrm{ms}^{-1}$, blue) on the Transmission Loss of a straight RTS with coiled cavities simulated by the TMM (plain) and a straight RTS simulated by the TMM (dashed) and by the RANS-SST/LNSE model (circles); the grey curves correspond to the no-flow case.

4.2 Convergent straight and coiled RTSs

A convergent design has been considered with a contraction factor $\kappa = 0.25$ such that axial variations of the Mach number cover the range of validity of Howe's model ($|M| < 0.3$). Stationary RANS-SST simulations on a fully-developed turbulent flow showed that a mean flow velocity of $6\ \mathrm{ms}^{-1}$ at $z = 0$ leads to an outlet mean flow velocity of about $100\ \mathrm{ms}^{-1}$ ($M(L) \approx 0.3$) at $z = L$. It is due to geometric acceleration of the mean flow, essentially when $z > L/2$, and weak sidebranch flow leakages.
In agreement with the trends discussed in in Sec. 4.1 as for the fully-opened RTSs, Figs. 6 and 7 show that DPC (resp. UPC) upshift (resp. downshift) the bandwidths of high dissipation and TL performance due to alteration of the cavity mouth reactance when the Mach number increases. The dissipation and TL values are generally higher under UPC compared to DPC, by up to 25% at 250 Hz on the dissipation of the CS RTS at 500 Hz (Fig. 4) and by up to 108 dB on the first TL peak of the CC RTS at 415 Hz (Fig. 5). DPC lead to over-damping of the cavity mouths, preventing acoustic inflow and efficient visco-thermal dissipation within the activated cavities, thereby resulting in enhanced transmission with respect to dissipation.

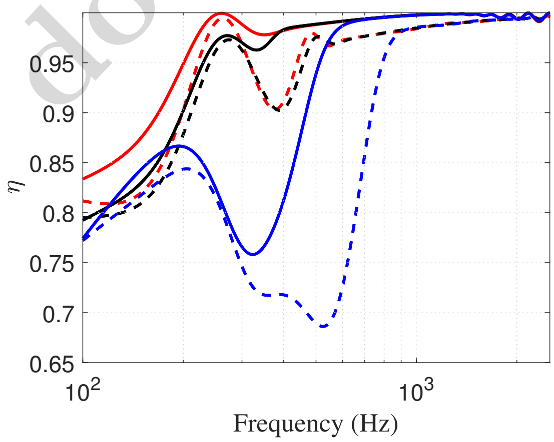

Figure 6. Influence of a low-speed flow ($U = -30\ \mathrm{ms}^{-1}$, red; $U = 30\ \mathrm{ms}^{-1}$, blue) on the dissipation spectra of a convergent RTS (dashed) and a convergent RTS with coiled cavities (plain) simulated by the TMM; the black curves correspond to the no-flow case.

The flow-induced alteration of the RTS wall impedance is predominant when $z > L/2$ towards the RTS outlet when the mean flow velocity takes its highest values. The largest alteration of the wall impedance occurs below 800 Hz for the CS RTS and below 600 Hz for the CC RTS when the quarter-wave resonances of the five deepest cavities are activated. This is clearly visible in Fig. 7 where UPC strongly enhance the TL peak value of the first quarter-wave resonance of CS and CC RTSs. In the range 1.5 – 1.8kHz and above 2 kHz, one observes mild grazing flow effects on the first-order quarter-wave resonances of the shallowest cavities of CC and CS RTSs, respectively, with reduced discrepancies of the dissipation and TL with respect to the no-flow case.

Figure 8 shows minute variations above 400 Hz of the specific input duct impedances, Z_{in}/Z_0, evaluated at the inlet of the CC RTS under UPC and DPC compared with the no-flow case. This confirms robustness of the impedance matching properties of the CC RTS despite large variations of the mean flow velocity across the silencer.

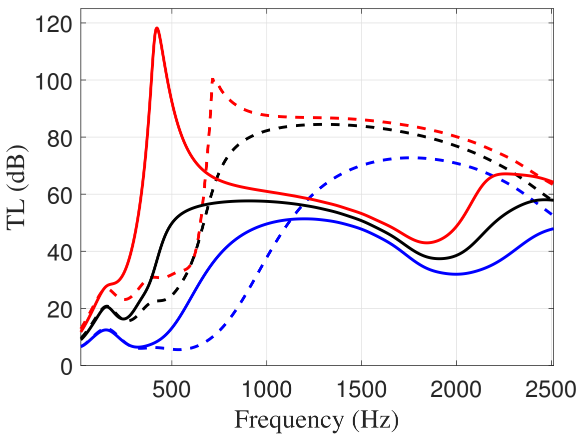

Figure 7. Influence of a low-speed flow ($U = -30\ \mathrm{ms}^{-1}$, red; $U = 30\ \mathrm{ms}^{-1}$, blue) on the Transmission Loss of convergent RTS (dashed) and a convergent RTS with coiled cavities (plain) simulated by the TMM; the black curves correspond to the no-flow case.

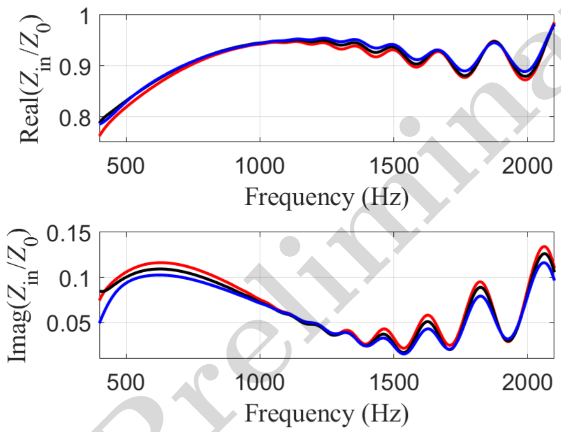

Figure 8. Influence of a low-speed flow ($U = -30\ \mathrm{ms}^{-1}$, red; $U = 30\ \mathrm{ms}^{-1}$, blue) on the input resistance (top) and reactance (bottom) of a convergent RTS with coiled cavities simulated by the TMM over the quarter-wave lateral resonance regime that extends between 400 Hz and 1100 Hz; the black curves correspond to the no-flow case.

4.3 Low-frequency RTS axial resonances

Below 400 Hz, Fig. 9 shows greater variation of the specific input impedance at the inlet of CC RTS compared with Fig. 8 above 400 Hz. It can be seen from the bottom subplot of Fig. 9 that the specific reactance equates zero at 260 Hz under UPC and no-flow condition whereas it crosses the frequency axis at 200 Hz under DPC. This corresponds to a resonant state well below the first quarter-wave resonance of the CC RTS deepest cavity.

Such resonances appear in Fig. 6 as a first maxima of dissipation for the CC RTS, reaching values of 0.99, 0.97 and 0.87 under UPC, no-flow and DPC. This hump of dissipation also occurs in Fig. 6 at similar frequencies for the power dissipated by the CS RTS. It is associated to the first axial half-wavelength resonance of the CC or CS RTSs with pressure-release boundary conditions at $z = 0$ and $z = L$, but with a reduced effective sound speed lower than c_0. Given an axial length $L = 0.15$ m, such axial resonance would occur towards 1.2 kHz if the slow sound effect was neglected. Such effect is due to axial variations of the wall impedance combined with reduction of the duct cross-section by the convergent profile. It amounts to an axially-averaged effective sound speed $c_{eff} = 78\ \mathrm{ms}^{-1}$ at 260 Hz under UPC and no-flow case, and to $c_{eff} = 60\ \mathrm{ms}^{-1}$ at 200 Hz under DPC.

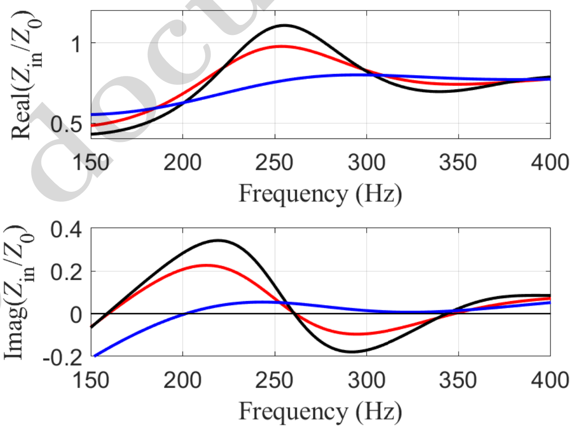

Figure 9. Influence of a low-speed flow ($U = -30\ \mathrm{ms}^{-1}$, red; $U = 30\ \mathrm{ms}^{-1}$, blue) on the input resistance (top) and reactance (bottom) of a convergent RTS with coiled cavities simulated by the TMM over the axial resonance regime; the black curves correspond to the no-flow case.

Similar variations of the mean flow magnitude produce an asymmetric variation of the effective sound speed, which is more pronounced under DPC with respect to UPC. Indeed, as seen in Fig. 1 ,the wall impedance of the cavities located at $z > L/2$ face the discharge flow associated to DPC (blue arrow), which is not the case for a suction flow associated to UPC (red arrow). As a consequence, DPC produce at low frequencies (below the lateral quarter-wave resonance frequencies) a much greater alteration of the wall reactance than UPC for both the CS and CC RTSs. This results in a greater decrease of the effective sound speed across the CC and CS RTS under DPC with respect to UPC. Figure 6 shows that the dissipation of convergent RTSs at this axial resonance is enhanced under UPC flow condition, but not under DPC. This axial resonance also generates a marked TL peak (Fig. 7) under UPC, but without noticeable effect under DPC.

5. Conclusions and perspectives

This study analyzed the robustness of fully-opened and flow-compliant convergent RTSs with straight or coiled cavities to UPC and DPC low-speed flow conditions. A transfer matrix formulation was developed to predict the dissipation and TL properties of the RTS, based on the cavity input impedances derived by Howe under low-speed grazing flow [9].

In the no-flow case, the TMM is validated against FEM results. it was shown that increasing the acoustical path length, particularly in the convergent design, progressively broadens and downshifts the high-dissipation plateau due to the merging of quarter-wave resonances and improved impedance matching. Among the tested designs, the CS and CC RTSs provide the widest efficiency bandwidths, with the CS configuration producing the highest TL peak at the first quarter-wave resonance of the deepest cavity.

The aero-acoustical performance of the four RTS configurations remains generally robust under low-speed grazing flow up to $30\,\mathrm{ms^{-1}}$, with limited degradation of dissipation efficiency, except under DPC at the low frequency axial resonance of the RTS. For the fully opened straight and coiled RTSs, grazing flow primarily induces frequency shifts of the high-dissipation plateau through flow-induced modifications of the cavity reactance. UPC systematically enhances the performance compared with DPC, yielding broader dissipation bandwidths and significantly higher TL levels, especially for the straight RTS. In contrast, DPC tends to over-damp the cavity mouth, thereby reducing the TL and narrowing the efficiency bandwidth, although maximum dissipation values remain largely preserved.

The convergent configurations (straight and coiled) exhibit similar trends but with amplified flow-induced alteration of the cavity impedance due to geometric acceleration of the mean flow over the second half of the convergent. Despite strong axial Mach number variations across the convergent RTS, impedance matching remains remarkably robust above 400 Hz. UPC again promotes higher dissipation and TL by maintaining a balanced loss-to-leakage ratio, whereas DPC induces over-damping at the cavity mouths. Stronger reduction of the effective sound speed at low frequencies results in the emergence of an axial half-wavelength resonance below 400 Hz due to slow-sound effects. At this resonance, dissipation under UPC remains largely preserved while being substantially degraded under DPC. Overall, the aeroacoustic performance of the rainbow trapping meta-liners at low Mach number will be enhanced if used in suction mode (UPC) rather than in discharge mode (DPC). These aeroacoustic performance have to be consolidated against measurements and Linearized Navier Stokes acoustic formulation coupled to RANS-SST fluid dynamic model under a low-speed fully-developed flow.

6. Acknowledgments

This work is part of the project PID2022-139414OB-I00 funded by MCIN/AEI/10.13039/501100011033/ and by "ERDF A way of making Europe". It has also been supported by the French government under the France 2030 investment plan, as part of the Initiative d'Excellence d'Aix-Marseille Université - A*MIDEX (AMX-22-RE-AB-157). We wish to thank the PSIVA platform of the Laboratoire de Mécanique et d'Acoustique for the use of its outstanding equipment.

References

[1] M. Yang and P. Sheng: "Sound absorption structures: from porous media to acoustic metamaterials," *Annual Review of Materials Research*, vol.47, pp. 83–114, 2017.

[2] G. Aydin and S. E. San: "Breaking the limits of acoustic science: A review of acoustic metamaterials," *Materials, Science and Engineering: B*, vol.305, 117384, 2024.

[3] N. Jimenez, V. Romero-Garcia, V. Pagneux and J.-P. Groby: "Rainbow-trapping absorbers: Broadband, perfect and asymmetric sound absorption by subwavelength panels for transmission problems," *Scientific Reports*, vol.7, 13595, 2017.

[4] Y. Aurégan, M. Farooqui and J.-P. Groby: "Low-frequency sound attenuation in a flow duct using a thin slow sound material," *The Journal of the Acoustical Society of America,* vol.139, no.5, pp. L149–L153, 2016.

[5] Y. Li and Y.S. Choy: "Broadband and low-frequency sound absorption of compact meta-liner under grazing flow," *Applied Acoustics,* vol.224, 110146, 2024.

[6] H.M. Yu and S.K. Tang: "Sound transmission across a narrow sidebranch array duct muffler at low Mach number," *The Journal of the Acoustical Society of America,* vol.148, pp. 1692–1702, 2020.

[7] C.J. Doolan: "Numerical Evaluation of Contemporary Low-Speed Wind Tunnel Contraction Designs," *ASME Journal of Fluid Engineering,* vol.129, pp. 1241–1244, 2007.

[8] T. Bravo and C. Maury: "Converging rainbow trapping silencers for broadband sound dissipation in a low-speed ducted flow," *Journal of Sound and Vibration,* vol.589, 118524, 2024.

[9] M.S. Howe: "The influence of grazing flow on the acoustic impedance of a cylindrical wall cavity," *Journal of Sound and Vibration,* vol.67, pp. 533–544, 1979.